BMC Genomics

RESEARCH Open Access

Environmental acclimatization of the relatively high latitude scleractinian coral *Pavona decussata*: integrative perspectives on seasonal subaerial exposure and temperature fluctuations

Man Zhang[1], Shan Huang[1], Li Luo[1] and Kefu Yu[1,2*]

Abstract

Background Coral reefs are being increasingly threatened due to global climate change. However, some coral species have shown strong tolerance despite living in marginal environments. The species *Pavona decussata* from Weizhou Island in the South China Sea experiences subaerial exposure in summer and winter due to extreme low tides, and their environmental acclimatization to this aerial exposure remains unexplored.

Results Here we aimed to explore the molecular mechanism of *P. decussata* under season or subaerial exposure background through physiological and multi-omics integrative analyses. Specifically, corals with a history of seasonal air exposure underwent comprehensive changes in energy metabolism and defense mechanisms compared to permanently submerged corals. In summer, corals experiencing subaerial exposure enhanced antioxidant defense by increasing the activities of the enzymes T-SOD and CAT, and the coral-associated bacterial community shifted toward the class Alphaproteobacteria that may have provided corals with resistance to environmental stresses. Moreover, the decrease in the transcript levels of the TCA cycle and the increase in metabolite content of ornithine suggested an alteration in energy metabolic pathways. Corals with an air-exposed background may have enhanced energy reserves in winter, as indicated by a higher content of Chl *a* and a rebound in coral-associated bacterial community toward the class Gammaproteobacteria. Furthermore, accumulation of the metabolite leukotriene D4 and activation of the TGF-beta signaling pathway suggested higher anti-inflammatory requirements and positive regulation by innate immunity.

Conclusions This study provides insights into the acclimatization of *P. decussata* to seasonal environmental fluctuations and demonstrates that relatively high-latitude corals possess the plasticity and acclimatory capacity to adapt to marginal environments.

*Correspondence:
Kefu Yu
kefuyu@scsio.ac.cn

Full list of author information is available at the end of the article

Keywords Scleractinian coral, *Pavona decussate*, Seasonal environmental fluctuations, Subaerial exposure, Temperature variation, Acclimatization

Background

The biodiversity of coral reefs provides diverse ecosystem services [1]. Scleractinian corals are the main frame-builders of coral reef ecosystems, comprising a mutually beneficial symbiosis with microorganisms such as zooxanthellae and bacteria [2]. Due to the complexity of coral holobionts, changes in environmental factors may lead to imbalances in the symbioses [3, 4], and the corals are then bleached or even threatened with death [5–7]. Therefore, in the context of coral habitat expansion driven by global warming [3], exploring the adaptive mechanisms by which corals survive under abiotic stress is critical to predicting their continued viability in changing environments.

Corals that survive in marginal marine habitats have attracted increasing attention as representing an alternative developmental state for corals in the face of environmental change [8]. In Hong Kong, the massive coral *Oulastrea crispata* is widely distributed along the highly urbanized coastline where there are vastly contrasting water quality conditions; yet, the coral showed continued environmental robustness [9]. Similarly, in the western fringing reef at Pulau Satumu, shallow reef communities surviving in highly turbid waters recovered quickly from acute thermal bleaching [10]. In Honolulu Harbor, the massive *Porites* corals living in shallow waters also exhibited greater bleaching resilience during several thermal stress events [11]. Furthermore, corals living in the intertidal and subtidal zones where environmental changes are more intense have been the focus of research in recent years. As sessile benthic organisms, corals are unable to move to seek shelter during tidal changes. Therefore, corals in intertidal and subtidal zones are often exposed at extreme low tides that exposes the corals to hypoxia, desiccation and UV stress and experience changes in temperature, salinity, and other environmental factors [12]. Such natural phenomena are commonly found in lower latitudes, for example, on Gorgona Island [13], Madura Island [14], Guam [15], Shell Island [16, 17], and the Pelorous and Orpheus Islands [18]. Corals in these habitats appear to be uniquely adapted to local environmental fluctuations. Similar to thermal bleaching, the branching coral genus *Acropora* and the family Pocilloporidae are susceptible to air exposure, while massive corals are the least affected [18]. An in situ simulation experiment on Gorgona Island in the tropical eastern Pacific demonstrated that extreme low tides were not lethal to the branching coral *Pocillopora damicornis* [13]. Thus, in the long term, studying how corals acclimate to air exposure may be able to provide insights into the future survival of corals in a changing climate.

Theoretically, under the effects of climate-induced stress, corals may migrate to higher latitudes where the range of seasonal temperature fluctuations is greater compared to tropical regions [19]. This serves to buffer the stress of abnormal environmental temperatures on corals, but also poses a new survival challenge for corals—how to cope with low winter temperatures. Further, air exposure and low winter temperatures can bring a double threat to corals. Hoegh-Guldberg et al. [20] reported that *Acropora aspera* from the Great Barrier Reef were exposed to unusually cold and dry air during subaerial exposure and suffered bleaching and mortality. This implies that the survival of corals under such marginal environmental conditions will depend on their ability to tolerate dynamic environments with more intense disturbances [21]. Therefore, understanding how relatively high-latitude corals acclimate to air exposure in wintry weather is essential for predicting the fate of corals. In general, acclimatization is achieved by a combination of differential gene expression by the coral host and the flexible composition of symbiotic microorganisms. Differential regulation of innate immunity and energy metabolism in coral hosts may reflect the results of acclimatization to distinct environments [22]. The coral-associated bacterial community may likewise be altered by the acclimatization process [23, 24]. Moreover, the metabolite profiles of corals after experiencing environmental changes could be used as signatures to reveal their adaptive history, and this would apply to an extended period following stress [25]. Studies that combine these characteristics will help provide insight into the acclimatization of corals to seasonal subaerial exposure.

Located in the relatively high latitude of the South China Sea, Weizhou Island has abundant coral resources, especially in the northern subtidal zone where there are large areas of *Pavona decussata*. Compared to tropical coral reef areas, Weizhou Island has a greater range of temperature variation, with a difference of up to 13.6 °C throughout the year [26], and the corals may thus be more tolerant to large temperature fluctuations [26]. Moreover, the subtidal *P. decussata* is periodically exposed to air due to extreme low tides in summer and winter. These corals may be acclimated to long-term seasonal environmental fluctuations. It is conceivable that the environmentally susceptible coral-associated bacteria and coral host gene regulation would allow *P. decussata* to survive under seasonal environmental fluctuations and that this would leave an associated metabolic history

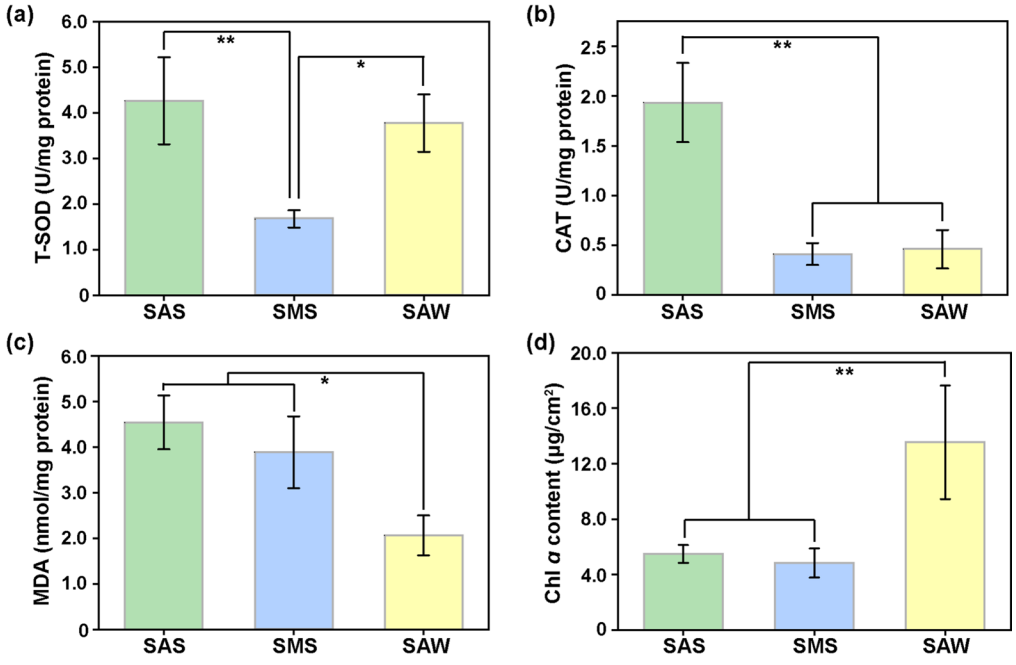

Fig. 1 The quantification of antioxidant capacity and Chl *a* content. (**a**) T-SOD, total superoxide dismutase. (**b**) CAT, catalase. (**c**) MDA, malondialdehyde. (**d**) Chl *a* content. Data are expressed as mean ± standard deviation (SD; $n=4$). U should be Unit. Significant differences were analyzed between groups (*$p<0.05$, **$p<0.01$)

Table 1 Alpha diversity statistics of coral-associated bacterial community

Estimators	SAS-Mean	SAS-SD	SMS-Mean	SMS-SD	SAW-Mean	SAW-SD	*p* value (SAS vs. SMS)	*p* value (SAW vs. SAS)
Ace	324.1	222.5	194.5	123.3	659.8	201.9	NS	**
Chao	319.1	219.6	192.2	121.1	657.1	200.7	NS	**
Sobs	316.6	217.7	191.4	120	651.6	199.1	NS	**
Shannon	3.64	1.38	1.58	1	4.01	1.04	**	NS
Simpson	0.15	0.12	0.53	0.3	0.14	0.15	**	NS

Note: Mean represented 'mean value', and the SD represented 'standard deviation'. NS represented 'non-significance', **$p < 0.01$

during long-term survival. Therefore, the research design incorporated: (1) quantification of antioxidant capacity and Chlorophyll *a* (Chl *a*) content; and (2) coral-associated bacterial diversity assessment, transcriptomic analysis, and metabolomic analysis. Assessing the survivability of *P. decussata* in seasonal environmental fluctuations is essential for understanding the plasticity of adaptive capacity under global climate change. This research will also enhance our understanding of coral stress tolerance at relatively high latitudes and provide a theoretical basis for future marginal reef conservation.

Results

Analysis of coral physiological indicators

The quantification of antioxidant capacity and Chl *a* content between different groups are shown in Fig. 1. In the experienced subaerial exposure in summer (SAS) group, the total superoxide dismutase (T-SOD) activity was significantly higher than that in the permanently submerged corals (SMS) group (Fig. 1a; $p<0.01$), with an increase of 155%. Similarly, the activity of the antioxidant enzyme catalase (CAT) in the SAS group was significantly higher from those in the SMS and SAW groups (Fig. 1b, $p<0.01$). Compared to the SMS group, the SAS group had a significant increase in CAT of about four times. The SAW group in winter had a significant 76% decrease compared to the SAS group in summer. In relative terms, the malondialdehyde (MDA) content of the SAW group was significantly lower than SAS group (Fig. 1c, $p<0.05$), with a decrease of 55%. Conversely, the Chl *a* content in the SAW group was significantly 147% higher than that in SAS group (Fig. 1d, $p<0.01$).

Dynamics of coral-associated bacterial communities

After 16S rRNA sequencing of 15 samples from the SAS, SMS, and SAW groups, 1,045,350 processed bacterial sequences were assigned to 12,306 amplicon sequence variants (ASVs), and the sequence details are presented in Additional file 2: Table S1. The statistics for alpha diversity are presented in Table 1. The Ace, Chao, and Sobs indices suggested no significant difference in community richness between the SAS and SMS groups, while

the richness of the SAW group was significantly higher than that of the SAS group ($p < 0.01$). In addition, the Shannon index reflecting community diversity was significantly higher for the SAS group than for the SMS group but was not significantly different from that of the SAW group. The Simpson index is inversely proportional to the Shannon index, and this indicated that the lowest diversity of coral-associated bacterial communities was in the SMS group. Overall, the SMS group had the lowest alpha diversity.

Based on the Bray-Curtis dissimilarity, principal coordinate analysis (PCoA) was used for demonstrating the variable characteristics of the coral-associated bacteria, with all samples being clustered and differentiated by groups (Fig. 2a). SMS group could be clearly distinguished from SAS and SAW groups on the PC2 axis. The dominant bacterial taxa in all three groups were similar, but their abundances were altered. At the phylum level, the main constituents of all three groups were Proteobacteria, Firmicutes, and Actinobacteriota (Fig. 2b). At the genus level, the top genera in relative abundance included BD1-7_clade, *Rhodopseudomonas*, and unclassified_k__norank_d__Bacteria in three groups (Fig. 2c). Moreover, linear discriminant analysis effect size (LEfSe) analysis identified differential microbial communities between groups, with alterations of the phylum Proteobacteria being mainly responsible for the differences in both SAS vs. SMS and SAW vs. SAS. Specifically, the SAS group has different compositions of the classes Alphaproteobacteria and Gammaproteobacteria

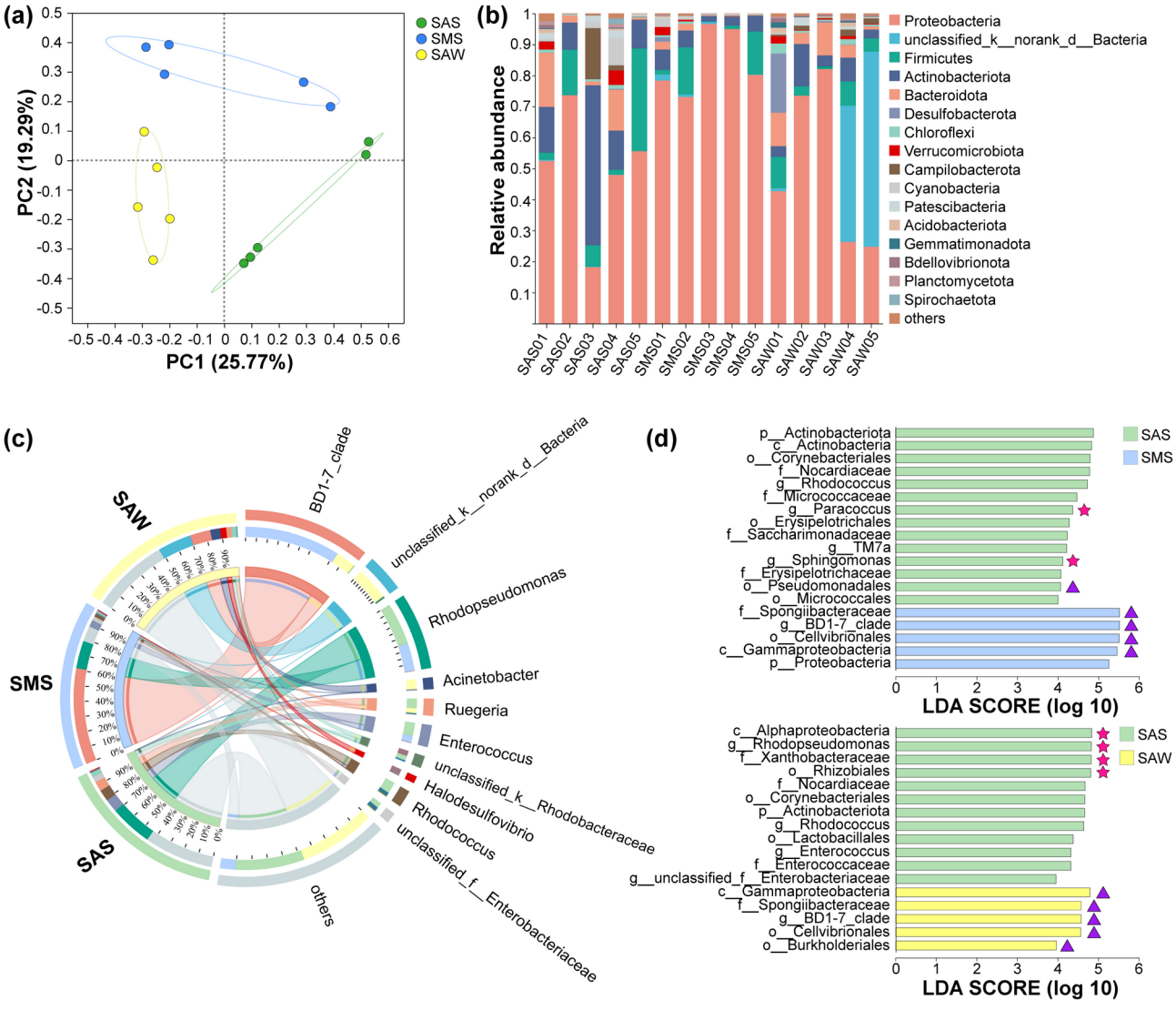

Fig. 2 The microbial beta diversity and community composition statistics. (**a**) PCoA analysis. (**b**) Microbial community composition at the phylum level. (**c**) Microbial community composition at the genus level between groups. (**d**) Statistics of taxa constituting differences between groups. The pink pentagrams marked taxa belonging to the class Alphaproteobacteria, and the purple triangles marked the counterparts of the class Gammaproteobacteria

compared to SAW and SMS groups (Fig. 2d). Relative to the SMS group, the relative abundance of the genus BD1-7 clade was lower in the SAS group, while the relative abundance of the genera *Paracoccus* and *Sphingomonas* was higher. Compared to SAS group, the relative abundance of the genus BD1-7 clade was elevated in the SAW group.

Different transcriptional responses of coral hosts

To determine the molecular mechanisms underlying the acclimatization of coral hosts to annual environmental changes, 12 samples from the SAS, SMS, and SAW groups were employed for RNA sequencing. In total, 583,925,222 clean reads were produced based on 592,968,090 raw reads, which were then assembled into 267,502 unigenes. The sequencing results are detailed in Additional file 3: Table S2. The analysis of molecular variance (AMOVA) results for single nucleotide polymorphism (SNP) loci are presented in Additional file 4: Table S3. There was minimal genetic differentiation between the groups (F_{ST} < 0.05, p < 0.05). Principal component analysis (PCA) plots revealed differences in expression

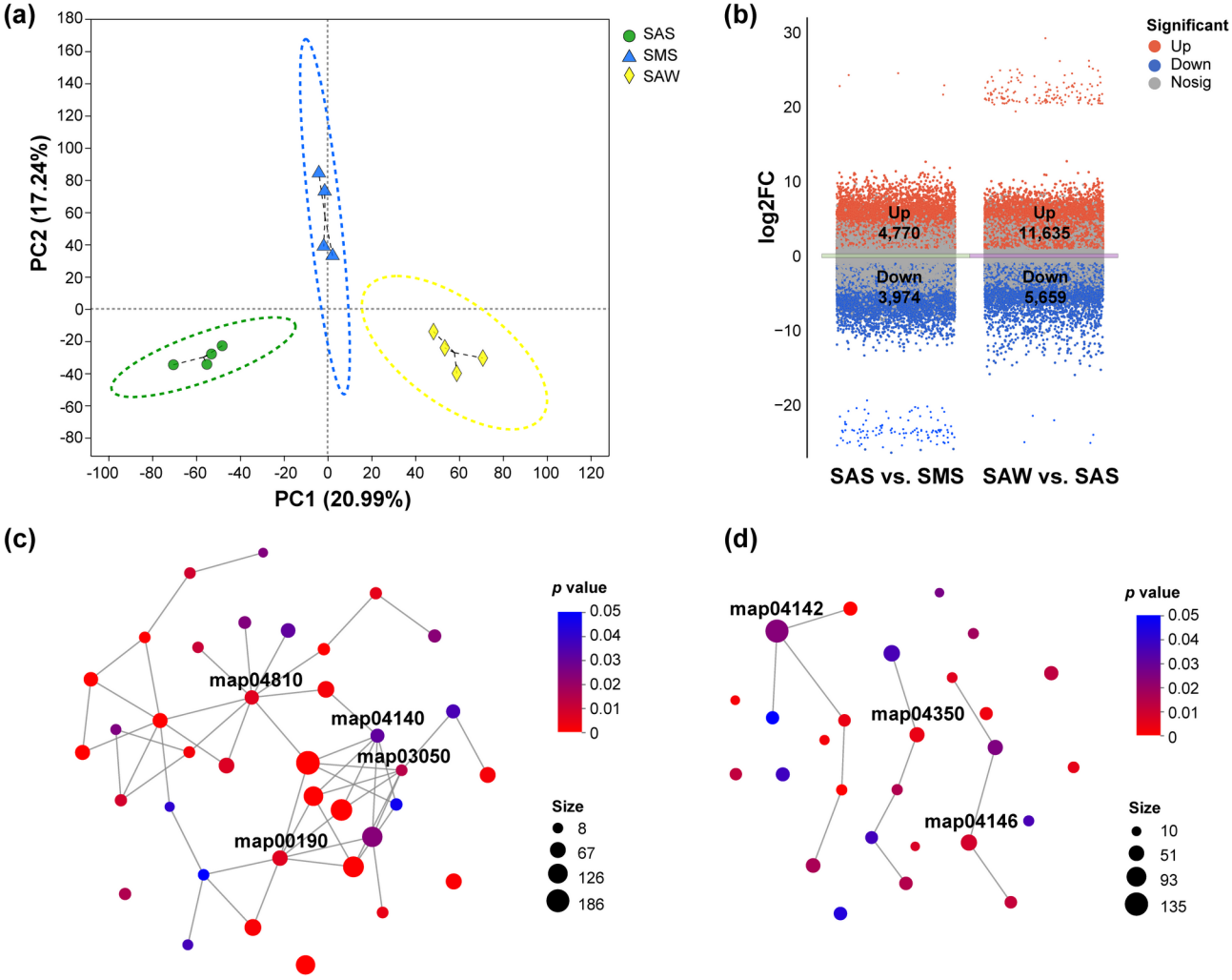

ID	Description
map04810	Regulation of actin cytoskeleton
map04140	Autophagy - animal
map03050	Proteasome
map00190	Oxidative phosphorylation

ID	Description
map04142	Lysosome
map04350	TGF-beta signaling pathway
map04146	Peroxisome

Fig. 3 Characterization and comparison of the transcriptional profiles. (**a**) PCA plot. (**b**) Scatter diagram demonstrating the DEGs for two different comparison schemes (SAS vs. SMS and SAW vs. SAS, the latter is considered the reference group). The FDR < 0.01 is indicated in red, while the FDR ≥ 0.01 is indicated in blue. The networks showed the core pathways of (**c**) SAS vs. SMS and (**d**) SAW vs. SAS. Each dot represented a pathway, and only the significant pathways are shown. The more DEGs enriched within the pathway, the larger the dot. Also, the color of the dot reflected the *p*-value. Only the names and map IDs of critical pathways are shown in the map

between the SAS and SMS groups, as well as between the SAW and SAS groups (Fig. 3a), with replicates showing higher correlation within groups and a clear separation between groups. Subsequently, unigenes with significant differential expression between groups were identified. There were 8,744 differentially expressed unigenes (DEGs) in the SAS group relative to the SMS group. In addition, compared to the SAS group, 17,294 DEGs were identified in the SAW group (Fig. 3b).

Gene Ontology (GO) annotation analysis indicated that these two sets of DEGs had similar functional classification. Among these, "cellular process" and "metabolic process" were the dominant subcategories in biological process. The "cell part" had the highest proportion in cellular component, while "binding" and "catalytic activity" were the most important in molecular function (Additional file 1: Fig. S2). The GO functions of these DEGs were enriched, and the top 20 significantly enriched ($p < 0.05$) GO terms in biological process reflected certain changes. Compared to the SMS group, the SAS group was significantly enriched in the subcategories of "cellular process" and "metabolic process", with the upregulation of terms belonging to "cellular process" such as "cilium movement (GO: 0003341)" and "cellular component assembly (GO: 0022607)" and the downregulation of terms belonging to "metabolic process" such as "respiratory electron transport chain (GO: 0022904)" and "peptide biosynthetic process (GO: 0043043)" (Additional file 1: Fig. S3a). Meanwhile, the SAW group was significantly enriched in "biological regulation" and "metabolic process" subcategories, and both showed upregulation compared to the SAS group; for example, this included "proteasomal protein catabolic process (GO: 0010498)", "organonitrogen compound catabolic process (GO: 1901565)", and "regulation of biosynthetic process (GO: 0009889)" (Additional file 1: Fig. S3b).

In the Kyoto Encyclopedia of Genes and Genomes (KEGG) pathway enrichment analysis, the DEG set of SAS vs. SMS was significantly enriched ($p < 0.05$) in 42 pathways, including "citrate cycle (TCA cycle) (map00020)" and "steroid biosynthesis (map00100)" (Additional file 5: Table S4). Figure 3c shows that four pathways, "regulation of actin cytoskeleton (map04810)", "oxidative phosphorylation (map00190)", "autophagy-animal (map04140)", and "proteasome (map03050)", had strong associations with other pathways. In contrast, the DEG set of SAW vs. SAS was significantly enriched in 27 pathways, including "biosynthesis of unsaturated fatty acids (map01040)" (Additional file 5: Table S4), with three pathways showing associations with other pathways, namely "lysosome (map04142)", "TGF-beta signaling pathway (map04350)", and "peroxisome (map04146)" (Fig. 3d).

Metabolomic profiling of *P. decussata*

The changes in the metabolome of *P. decussata* under different environmental conditions were analyzed using LC-MS. After forming the data matrix, a total of 1,889 variables were identified in positive (POS) ionization mode and 1,248 in negative (NEG) mode, which were preprocessed to obtain metabolite quantities. A total of 1,741 metabolites were identified in POS mode and 1,152 metabolites in NEG for all samples. The number of metabolites identified accounted for 92.17% and 92.31% of the number of variables in the POS and NEG models, respectively. After data processing, the partial least squares discriminant analysis (PLS-DA) score plot showed significant differences in metabolites in both POS and NEG modes (Fig. 4a and b). Subsequently, an orthogonal partial least squares discriminant analysis (OPLS-DA) model was used to discriminate the significantly different metabolites (DMs). In both POS and NEG modes, 54 DMs were obtained for SAS vs. SMS (Fig. 4c), and 825 DMs were obtained for SAW vs. SAS (Fig. 4d).

Upon analyzing the KEGG metabolic pathway information for these DMs (Additional file 6: Table S5), the majority in both groups were involved in two categories of energy supply pathways, "amino acid metabolism" and "lipid metabolism" (Additional file 1: Fig. S4). A topological pathway analysis identified two significantly enriched pathways in SAS vs. SMS, namely "arginine biosynthesis (map00220)" and "arginine and proline metabolism (map00330)" (Fig. 4e). Both pathways contained the upregulated metabolite ornithine (Additional file 1: Fig. S5a) associated with amino acid metabolism. In SAW vs. SAS, five significantly enriched pathways were identified, namely "arginine and proline metabolism (map00330)", "glycerophospholipid metabolism (map00564)", "arginine biosynthesis (map00220)", "nucleotide metabolism (map01232)", and "arachidonic acid metabolism (map00590)" (Fig. 4f). In contrast, the abundance of metabolite ornithine decreased in SAW group compared to SAS group. The metabolite leukotriene D4 of "arachidonic acid metabolism (map00590)" associated with lipid metabolism was upregulated in SAW vs. SAS (Additional file 1: Fig. S5b).

Association analyses of transcriptome and metabolome

The O2PLS model was fitted to the DEGs and DMs of SAS vs. SMS and SAW vs. SAS. The contributions of each part showed that both SAS vs. SMS and SAW vs. SAS had high contributions of their "Joint part", ranging from 86.55 to 100.00% of "Joint part and Orthogonal part" individually (Additional file 7: Table S6), indicating that the model could be used to explain the joint variation in the transcriptome and metabolome. Furthermore, the joint loadings plot showed the extent to which each

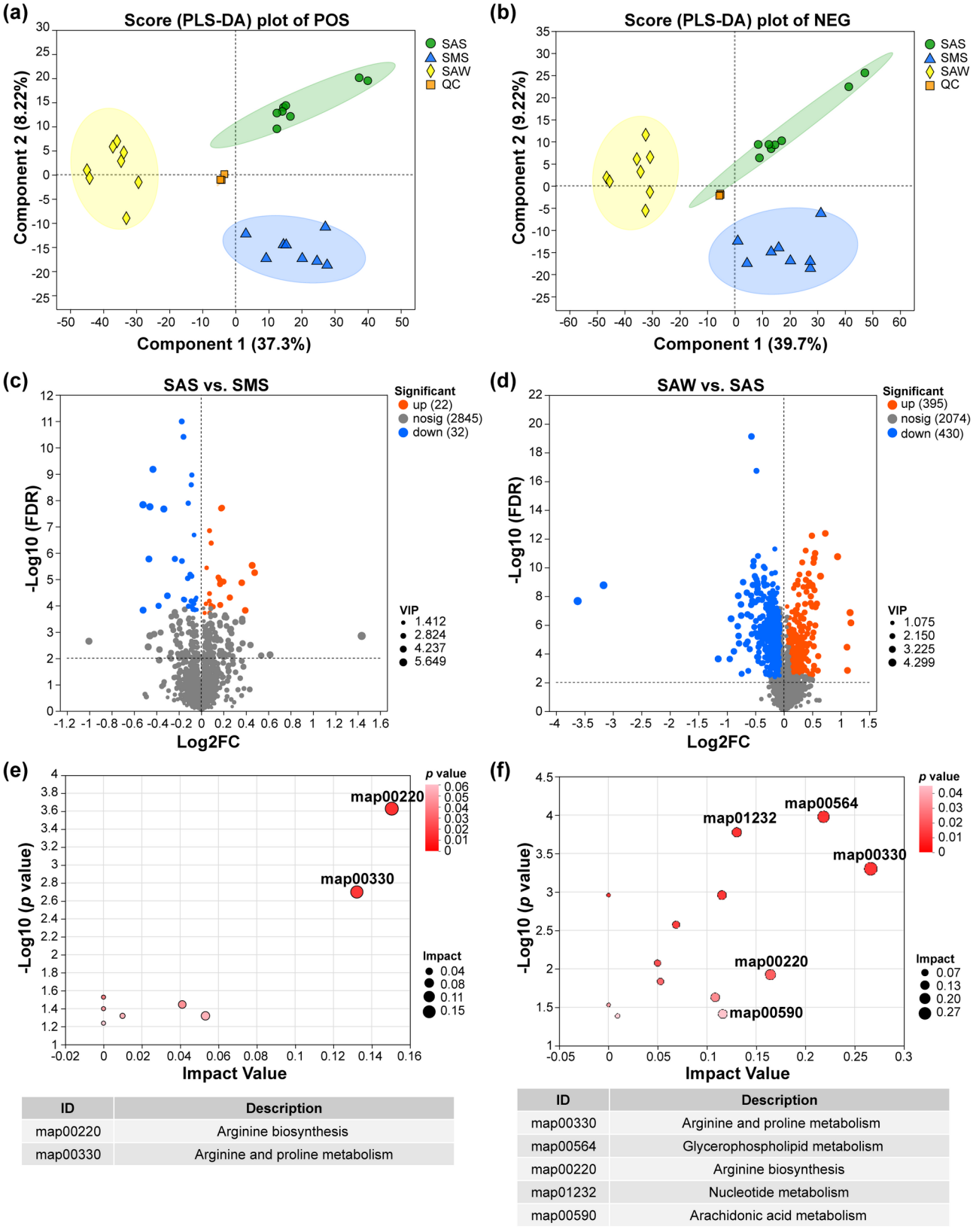

ID	Description
map00220	Arginine biosynthesis
map00330	Arginine and proline metabolism

ID	Description
map00330	Arginine and proline metabolism
map00564	Glycerophospholipid metabolism
map00220	Arginine biosynthesis
map01232	Nucleotide metabolism
map00590	Arachidonic acid metabolism

Fig. 4 Characterization and comparison of the metabolite profiles. PLS-DA analysis of individual samples in (**a**) POS mode and (**b**) NEG mode. The volcano plots showed the DMs of (**c**) SAS vs. SMS and (**d**) SAW vs. SAS. The key pathways in (**e**) SAS vs. SMS and (**f**) SAW vs. SAS were shown. The key pathways are labelled in terms of impact value. The larger the impact value, the more important the pathway. Only the top five pathways in (**f**) are labelled

variable in one omics approach was associated with the other omics in two dimensions, with larger absolute values indicating stronger associations. In this study, both SAS vs. SMS (Additional file 1: Fig. S6a and Fig. S6b) and SAW vs. SAS (Additional file 1: Fig. S6d and Fig. S6e) had strong correlations between almost all the variables among muti-omics.

To further explore the main mechanisms of transcriptional and metabolic regulation in the corals with a seasonal air-exposed background, the pathways concerning energy metabolism and innate immunity were selected from the above enrichment results for correlation analysis (Additional file 8: Table S7). The strong correlations between gene expression and metabolite abundances in these pathways are shown in Additional file 1: Fig. S7. In the SAS vs. SMS comparison, ornithine was an important metabolite based on the above omics analyses, and it was significantly negatively correlated with the rate-limiting enzymes citrate synthase (*CS*) and isocitrate dehydrogenase (*IDH*), which were downregulated in "citrate cycle (TCA cycle) (map00020)" (Fig. 5a). In the SAW vs. SAS comparison, leukotriene D4 was enriched as a key metabolite, and it was significantly positively correlated with genes related to "arachidonic acid metabolism (map00590)" and with bone morphogenetic protein receptor, type I (*BMPRI*), bone morphogenetic protein (*BMP*) and SMAD family member 4 (*SMAD4*), which were upregulated in "TGF-beta signaling pathway (map04350)" (Fig. 5b).

Discussion

Physiological plasticity of *P. decussata* in response to variable environmental stress

P. decussata has shown strong tolerance to environmental stress [7, 26], and this may be reflected at the physiological level in the present study. The potential of *P. decussata* to acclimatize to air exposure included stronger activities of the antioxidant enzymes T-SOD and CAT (Fig. 1a and b), acclimatization that may be beneficial in eliminating reactive oxygen species (ROS) generated by dramatic environmental changes [27, 28]. Moreover, free radicals react with lipids to form MDA [29], and thus the lower MDA content may be indicative of a decreased oxidative response in *P. decussata* that experienced air exposure in winter. Meanwhile, the higher Chl *a* content in the SAW group (Fig. 1d) could also provide stronger photoprotection through the xanthophyll cycle of zooxanthellae [30], resulting in a reduction of potential existential threats during the winter months.

Coral-associated bacterial communities may be involved in the acclimatization

Coral-associated bacterial communities play key roles in coral health, disease, and evolution due to the fact that their habitats are closely linked to host tissue structures [31–34]. Thus, coral-associated bacteria are vulnerable to environmental variation, and the corresponding changes in their composition may in turn affect the coral hosts [35]. Previous studies have shown that the alpha diversity of coral-associated bacteria increases to a certain

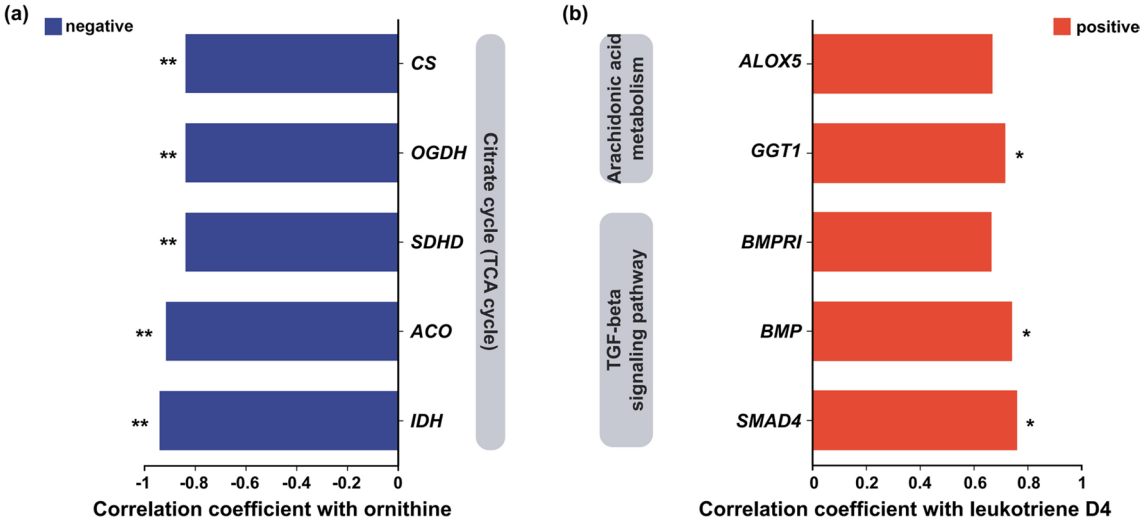

Fig. 5 The correlation plot between the expression of key genes and the abundances of core metabolites. The left chart reflected the correlation between metabolite ornithine and genes associated with the citrate cycle (TCA cycle) in (**a**) SAS vs. SMS, and the right chart represented the correlation between metabolite leukotriene D4 and genes related to the arachidonic acid metabolism and TGF-beta signaling pathway in (**b**) SAW vs. SAS. The blue bars represented negative correlations and red represented positive. The horizontal coordinate showed the correlation coefficient. Significance of differences was indicated by $*p < 0.05$ and $**p < 0.01$. *CS*, citrate synthase; *OGDH*, oxoglutarate dehydrogenase; *SDHD*, succinate dehydrogenase complex subunit D; *ACO*, aconitate hydratase; *IDH*, isocitrate dehydrogenase; *ALOX5*, arachidonate 5-lipoxygenase; *GGT1*, leukotriene-C4 hydrolase; *BMPRI*, bone morphogenetic protein receptor, type I; *BMP*, bone morphogenetic protein; *SMAD4*, SMAD family member 4

extent under external stresses [36, 37], contributing to the symbiont's resistance to infections and the maintenance of essential functions of the microbiota [26]. In our research, both the SAS and SAW groups that experienced subaerial exposure showed higher alpha diversity of coral-associated bacteria than the always-submerged SMS group (Table 1). The sensitive changes in coral-associated bacterial community diversity may indicate that the disturbance from air exposure is a potential stressor for *P. decussata* both in summer and winter. Interestingly, the community richness indices Ace, Chao, and Sobs were significantly higher in the SAW group compared to the SAS group, in contrast to previous findings on *P. decussata* [26]. This indicated that *P. decussata* may be also highly tolerant to air exposure in winter. Additionally, our results showed that the microbial communities of the samples that were influenced by extremely low tides showed intercolonial variability, and the degree of variability varied between samples from different seasons (Fig. 2a). This implied that despite having the same coral host, there were effects of different environments on the microbiomes.

In this study, *P. decussata* experiencing subaerial exposure showed a decrease in the relative abundance of class Gammaproteobacteria and an increase in class Alphaproteobacteria in the SAS group relative to the SMS group (Fig. 2d). Unsurprisingly, the current study suggested that most bacteria that confer benefit to the symbiont belonged to the classes Gammaproteobacteria and Alphaproteobacteria [38], and the shift in these classes in coral-associated bacteria may be based on environmental acclimatization. The BD1-7 clade that carries out carotenoid biosynthesis [39] has been detected in corals and other marine organisms [26, 40]. The biosynthetic process is crucial for symbiont health [41]. *Paracoccus* sp. was demonstrated to be able to kill harmful bloom-forming algae [42], showing the potential for application in regulating environmentally harmful factors. Moreover, it has been shown that *P. marcusii* can produce ROS-reactive pigments to help detoxify free radicals and ROS [43]. In addition, a metabolic characteristic of the genus *Sphingomonas* is the capacity for xenobiotic degradation, an ability that may play an essential role in adaptation to oligotrophic marine environments [44]. Therefore, the switch from class Gammaproteobacteria (genus BD1-7 clade), which may favor the maintenance of a stable healthy state of the coral host, to class Alphaproteobacteria (genera *Paracoccus* and *Sphingomonas*) that are resistant to exogenous stresses may be microbiological evidence that *P. decussata* was affected by air exposure and acclimatized to this stress. In addition, compared to SAS group, the relative abundances of some bacteria from the class Gammaproteobacteria was elevated after air exposure in winter (Fig. 2d). The genus BD1-7 clade played a key role in energy utilization [26]. This suggested that coral-associated bacterial communities may assist *P. decussata* in acclimatizing to environmental fluctuations during winter by shifting to structures that favored symbiont energy reserves.

Overall, changes in the diversity of coral-associated bacterial communities, along with differences in bacterial taxa, allowed the coral host to cope with stresses in different conditions, suggesting that *P. decussata* may be resistant to external pressures due to the presence of the symbiont.

Coral hosts responded to environmental stresses through flexible gene regulation

Extensive studies on scleractinian corals have shown that energy metabolism and homeostasis are closely linked under exogenous stresses [4, 45, 46]. The citrate acid cycle, also known as the TCA cycle, was a conserved primitive metabolic pathway typically serving as the organism's energy engine [47]. We noted that the "citrate cycle (TCA cycle) (map00020)" pathway was significantly enriched in SAS vs. SMS. In this pathway, *CS* and *IDH* were both downregulated in the SAS group, suggesting that air exposure limited the TCA cycle and affected the efficiency of energy utilization in the coral host. The result was consistent with that of previous studies on the response of coral hosts to exogenous stresses [4, 48]. Moreover, the "peroxisome (map04146)" pathway was enriched in the SAW vs. SAS comparison (Fig. 3d), possibly dominating more abundant amino or fatty acid metabolism and regulating the level of ROS [49]. This may be a survival advantage for *P. decussata* in response to extremely low tides in winter.

P. decussata has demonstrated remarkable resilience to thermal stress, as evidenced by having flexible regulation of the antioxidant response and innate immunity [7]. Specifically, proteasomes are protease complexes that selectively degrade short-lived regulatory or damaged proteins [50]. To maintain homeostasis during oxidative stress in the organism, ubiquitinated proteins are degraded by the proteasome as a general damage signature [51]. In this study, the "proteasome (map03050)" pathway were enriched in the SAS group relative to the SMS group (Fig. 3c). Moreover, autophagy is an essential component of cellular response to stress [52] as a type of programmed cell death pathway [53] and can be activated by oxidative stress [54]. In the SAS vs. SMS comparison, the "autophagy-animal (map04140)" pathway (Fig. 3c) may reveal plasticity in gene expression after stimulation by subaerial exposure. Additionally, in the SAW group, the activated "lysosome (map04142)" pathway (Fig. 3d) may have been used to control oxidative stress [28], similar to the activated "peroxisome (map04146)" pathway. Therefore, we hypothesized that *P. decussata*

experiencing seasonal subaerial exposure may respond to oxidative stress in different ways. In summer, individuals that were consistently submerged may maintain cellular homeostasis through ubiquitinated protein degradation by proteasomes, whereas their counterparts that experienced subaerial exposure may protect cells through enhanced antioxidant T-SOD and CAT enzyme activities and activation of autophagy. In winter, *P. decussata* that experienced air exposure maintained high antioxidant enzyme (T-SOD) activity and may further cope with oxidative stress through lysosomes. Ultimately, there was no significant difference in the extent of oxidative damage between SAS and SMS groups (Fig. 1c), reflecting the effectiveness of gene regulation in *P. decussata* with subaerial exposure in summer. In addition, the corals in winter may have a significant reduction in the degree of oxidative damage (Fig. 1c) due to the combined action of their antioxidant enzymes and organelles.

Innate immunity seems to play an essential role in the response of *P. decussata* to air exposure. As a form of innate immunity [55], autophagy could be activated when the coral host is stressed and challenged, as shown in the SAS group. Similar results have been observed in tolerant *Porites* species [56]. In addition, *BMPRI*, *BMP* and *SMAD4* in "TGF-beta signaling pathway (map04350)" was upregulated in the SAW group relative to the SAS group. It is known that the TGF-beta signaling pathway can act as an innate immune pathway as an enforcer of immune tolerance and an inhibitor of inflammation [57]. In *P. decussata*, the anti-inflammatory effect of the TGF-beta signaling pathway may be beneficial for maintaining organismal health during air exposure in winter. It follows that *P. decussata* defends against threats from subaerial exposure by regulating the innate immune-related pathways, both in summer and winter; this may be a clue to its resilience.

In summary, the flexible gene regulation capacity of *P. decussata* may be a necessary asset for its survival in changing environmental conditions, which either directly or indirectly impacted its basic physiological processes.

Altered metabolic profiles may reflect the stress history of *P. decussata*

The metabolome results for both SAS vs. SMS and SAW vs. SAS showed that the enriched KEGG pathways contained "arginine biosynthesis (map00220)" and "arginine and proline metabolism (map00330)" on amino acid metabolism (Fig. 4e and f). This implied that the changes in amino acid metabolism may be a sensitive reflection of coral responses to environmental changes, and the same results were also found in the metabolic profiles of corals undergoing thermal stress [58]. Scleractinian corals absorb and utilize nitrogen for growth and development under stable conditions, including their most representative calcification. Previous studies have demonstrated that urea may be an important source of nitrogen for corals [59–61] and that the urea cycle is also involved in calcification in scleractinian corals [62]. In this study, the changes in the above two pathways focused on ornithine, an intermediate molecule in the urea cycle that is also an essential substrate for proline synthesis [63]. Compared to the SMS and SAW groups, the upregulation of ornithine in the SAS group (Additional file 1: Fig. S5) predicted a stronger material basis for the urea cycle. Additionally, *P. decussata* that experienced air exposure may have a stronger capacity for calcification in summer, consistent with the findings from other reef-building corals [64–67], suggesting that subaerial exposure may not affect classic seasonal patterns of coral calcification.

In the present study, changes in lipid metabolism such as "glycerophospholipid metabolism (map00564)" and "arachidonic acid metabolism (map00590)" were observed in the SAW vs. SAS comparison (Fig. 4f). Two types of metabolites phosphatidylcholine (PC) and phosphatidylserine (PS) in "glycerophospholipid metabolism (map00564)", which usually serve as typical cnidarian lipids [68], were upregulated in SAW vs. SAS (Additional file 1: Fig. S5b). These lipids comprise the major lipid structures in eukaryotic cell membranes, suggesting that *P. decussata* with a history of air exposure ultimately may acclimat to winter by improving membrane fluidity to help maintain cellular function [69]. Similarly, arachidonic acid, which can be used as an indicator to evaluate coral health [70], indicated physiological changes in *P. decussata* experiencing subaerial exposure and low temperatures during winter. In "arachidonic acid metabolism (map00590)" pathway, the downstream catabolic product leukotriene acts as an inflammatory mediator to trigger or participate in inflammatory responses [71]. In our metabolome results, leukotriene D4 was upregulated in the SAW group relative to the SAS group (Additional file 1: Fig. S5b), suggesting that *P. decussata* experiencing air exposure may have a higher risk of inflammation in winter.

Taken together, the changes in amino acid and lipid metabolism may be historical signatures of seasonal environmental fluctuations experienced by *P. decussata* and may further reveal the variation in biological processes in different seasons. These findings were essential for our comprehensive assessment of the acclimatization of *P. decussata*.

Integrated evaluation of the acclimatization and survival potential of *P. decussata* to marginal environments

The future of coral reefs depends on the ability of reef-building corals to respond to rapid environmental changes [72]. In this study, in addition to the flexible

coral-associated bacterial communities, *P. decussata* with a history of seasonal air exposure had apparent physiological advantages in antioxidant and photosynthetic capacity (Fig. 6). Subsequent O2PLS models successfully fitted transcriptomic and metabolomic data and revealed strong correlations (Additional file 1: Fig. S6), implying a link between gene regulation and metabolite abundances. Further analyses found that similar to other scleractinian corals [4, 54], *P. decussata* from Weizhou Island located in a subtropical marginal coral reef responded to stress through alterations in energy metabolism and innate immunity. Thus, these changes could be used to assess the acclimatization and survival potential of *P. decussata* under varied environmental conditions.

In general, coral-associated microbes have shorter generation times compared to coral hosts, implying that they may acclimatize more rapidly and provide corresponding adaptive capacity to the corals [72]. Thus, changes in bacterial community structure and diversity under different conditions [24, 73] have been evaluated in previous studies of coral acclimatization and adaptation [72]. Similar to our findings, the coral-associated bacterial community was altered at the genus level on Madura Island reefs where cyclical subaerial exposure also occurred, although Proteobacteria was still the dominant phylum [13]. Both at low and relatively high latitudes, these results demonstrated the involvement of coral-associated bacteria in the ongoing effects caused by subaerial exposure. Their specific alterations may contribute to coral stress resistance and energy reserves (Fig. 6), although the exact mechanism of bacteria in the acclimatization of corals to seasonal environmental fluctuations remains unclear. For coral hosts, the degree of genetic differentiation among populations can be assessed to evaluate the impacts of environmental fluctuations. In this study, the low yet statistically significant level of genetic differentiation among populations may suggest adaptation of the *P. decussata* coral host to tidal-induced environmental fluctuations at Weizhou Island. However, due to the small sample size and the limitations of RNA-seq, the interpretation of F_{ST} value may lack comprehensiveness, necessitating further validation.

Additionally, the level of energy metabolism in the coral host is closely linked to the stress response process. In previous studies, energy allocation by corals was the basis for acclimatization [12, 74]. In this research, compared to the SMS group, the TCA cycle pathway in the SAS group was downregulated, while the activities of antioxidant enzymes T-SOD and CAT, proteins containing a large number of amino acid residues [75], were significantly increased (Fig. 6). These phenomena may indicate that *P. decussata* with a subaerial exposure history may reduce the efficiency of energy utilization and allocate energy to the antioxidant system in summer. In contrast, the negative correlation between the abundance of the metabolite ornithine in the urea cycle and the gene expression of *CS* and *IDH* in the TCA cycle (Fig. 5a) may point to some degree of substance flow between the two pathways. Theoretically, the urea cycle and the TCA cycle are connected by aspartic acid and fumarate, i.e.,

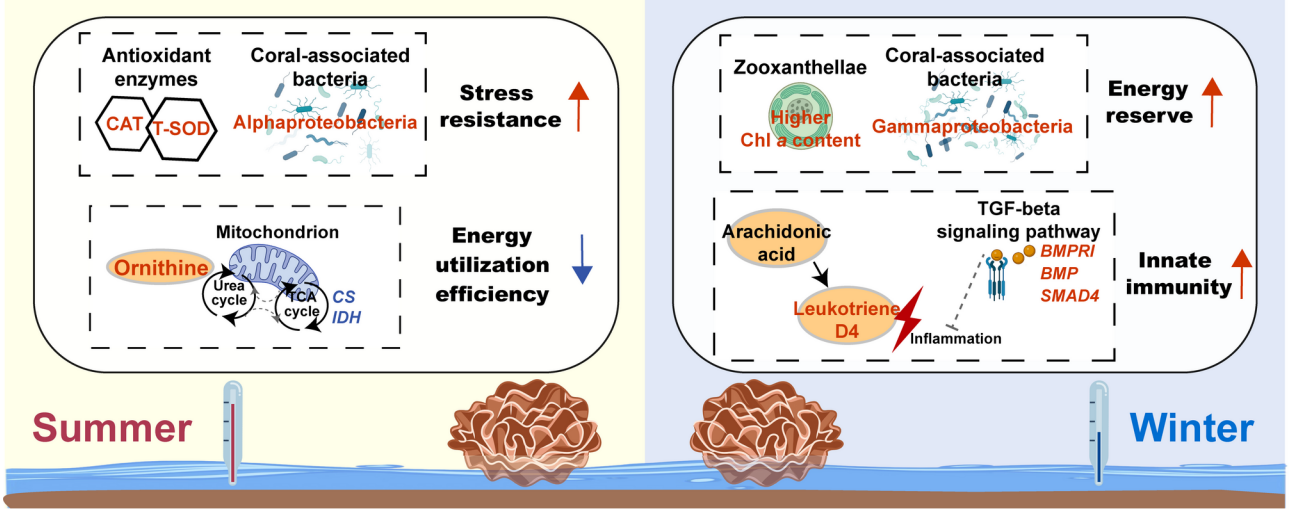

Fig. 6 Overview of the subtidal *P. decussata* acclimatization to seasonal subaerial exposure and temperature fluctuations. The left half of it depicted changes in corals with an exposure history during the summer relative to those without exposure backgrounds, and the right half detailed the variations of corals which experienced subaerial exposure under cold temperature conditions in winter. Characters in italics represented genes, and characters on the orange oval and white hexagonal icons represented substances. Red font and arrows indicated up-regulation or increase, while blue font and arrows indicated down-regulation or decrease. The black arrows denoted the direction of the response and the dotted lines signified presumptions. CAT, catalase; T-SOD, total superoxide dismutase; *CS*, citrate synthase; *IDH*, isocitrate dehydrogenase; *BMPRI*, bone morphogenetic protein receptor, type I; *BMP*, bone morphogenetic protein; *SMAD4*, SMAD family member 4

oxaloacetate from the TCA cycle synthesizes aspartic acid and then participates in the urea cycle, while fumarate produced by the urea cycle enters the TCA cycle [76, 77]. In our metabolome data, the active urea cycle indicated by ornithine may be a surrogate program for the TCA cycle due to the reduction of energy utilization efficiency (Fig. 6), although neither aspartic acid nor fumarate was detected, possibly due to detection errors. Thus, *P. decussata*, similar to other corals that experience subaerial exposure [12], has certain energy adjustment strategies to cope with high temperatures and air exposure in summer, and such advantages may allow the corals to survive.

Higher Chl *a* content favored coral photosynthesis, in turn facilitating resistance to environmental stress [78]. In this research, *P. decussata* with an air-exposed background possessed a higher Chl *a* content in winter, indicating the resistance to marginal environments at relatively high latitudes and an energy advantage (Fig. 6). At low temperatures, innate immunity is thought to benefit corals to adapt to environmental stresses [26, 54], and the same result was obtained in our study. *P. decussata* emerged from the sea surface for hours and then became submerged in cold seawater, and this may cause abnormalities in lipid metabolism such as an increase in leukotriene D4 indicative of the high risk of inflammation. In addition, the abundance of leukotriene D4 was positively correlated with the expression of *BMPRI*, *BMP* and *SMAD4* related to the TGF-beta signaling pathway (Fig. 5b), demonstrating that innate immunity functions in *P. decussata* to prevent inflammatory responses and maintain homeostasis in winter (Fig. 6).

In general, the adaptive capacity of corals to extreme environments has been closely linked to taxa [79], similar to thermal bleaching events [80, 81]. The leaf coral *P. decussata*, an intermediate between branching and massive corals, may have innate tolerant and adaptive advantages. Additionally, due to the geographical advantage of relatively high latitudes, similar to north-western Australia and in Reunion Island [82, 83], most air exposure on Weizhou Island occurs at sunrise or sunset, a factor that may have protected *P. decussata* from prolonged exposure to the sun and the threat of high temperatures, allowing this species to continue to survive after the seasonal subaerial exposure. Overall, biotic and abiotic factors have allowed *P. decussata* to successfully acclimatize to seasonal environmental fluctuations in Weizhou Island.

Conclusions

Scleractinian coral possess the potential to survive in marginal environments. Multi-omic analyses highlighted that coral-associated bacterial community structure and diversity of *P. decussata* on Weizhou Island changed in a direction that favored coral survival under seasonal subaerial exposure and temperature fluctuations. In addition, dynamic changes in energy metabolism and innate immunity were beneficial for maintaining coral homeostasis. To conclude, our analysis has contributed to a deeper comprehension of coral persistence in environmental fluctuations and provides a theoretical basis for future acclimation of relatively high-latitude corals.

Methods

Sample collection

The study site was located at Weizhou Island on the northern edge of the South China Sea (Fig. 7a). Field surveys in the northern part of Weizhou Island found that *P. decussata* surviving in the Blue Bridge area (21°4.16′N, 109°5.79′E) were exposed to recurrent extreme low tides (http://global-tide.nmdis.org.cn/default.html) in summer (June–August) and winter (December–February next year), similar to subtidal corals in other areas [16]. Such extreme low tides typically occurred around sunrise and lasted almost 3 h in summer. In winter, such tides occurred around sunset and lasted for about 3 h (Additional file 1: Fig. S1; Fig. 7b). These events usually occurred in succession, and at least three consecutive occurrences were observed during most of the summer and winter months. The sampling began at approximately 2 weeks after the end of consecutive extreme low tide events. We collected samples from corals that experienced subaerial exposure (SAS) by scuba diving on 28 August 2022. The seawater had a temperature of 30.3 °C and a salinity of 34.2 PSU, while the air had a temperature of 33.8 °C and a relative humidity of 57.6%. At the same time, we collected samples of permanently submerged corals (SMS) in water depths of approximately 3 m located at the same sampling sites. Similarly, we collected coral samples with a subaerial exposure background in winter (SAW) at the same sampling site on 3 March 2023. The seawater was recorded with a temperature of 20.4 °C and a salinity of 33.0 PSU, and the air conditions were noted as 21.0 °C in temperature and 52% in relative humidity. The distance between the SAS/SAW and SMS groups is approximately 10 m. Samples from eight different colonies were taken as 2–4 cm patches using hammers and chisels and as far away as possible to ensure that more comprehensive biological information was obtained. The samples were then rinsed with 0.22-μm filtered seawater to prevent contamination. Ultimately, all samples were quickly frozen in liquid nitrogen and stored at − 80 °C.

Physiological measurements

A total of 12 samples (four samples of each group) were used for quantifying the antioxidant capacity and

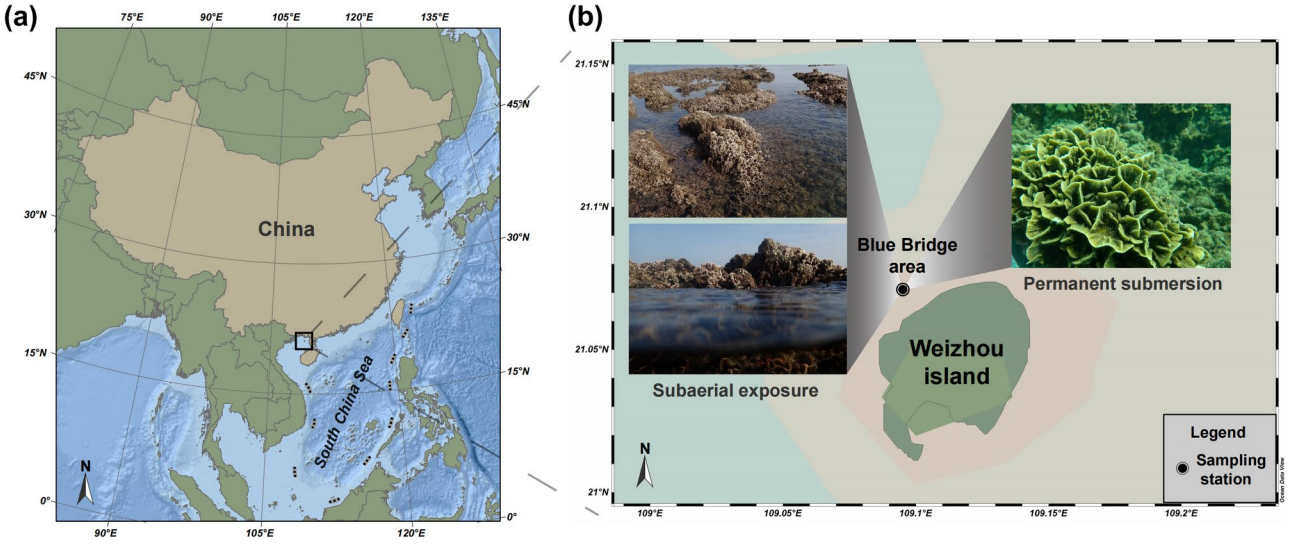

Fig. 7 The location map of sampling sites. (**a**) Weizhou Island in the South China Sea. (**b**) The image on the left showed that *P. decussata* in Blue Bridge area experienced subaerial exposure during extreme low tide event on 5 January 2022, and the image on the right showed their permanently submerged counterparts

Chl *a* contents of the corals. As previously described, a WaterPik® Ultra Water Jet (Water Pik, USA) filled with 0.22-μm filtered seawater was used to remove the coral tissue from the skeleton [84]. After obtaining coral tissue homogenates, three subsamples were taken from each replication. Then, the coral tissue homogenate supernatant was used to analyze the antioxidative indicators. The activities of total superoxide dismutase (T-SOD) and catalase (CAT) and the content of malondialdehyde (MDA) were assayed using commercial kits (Nanjing Jiancheng Bioengineering Institute, China). The total protein was measured using a quantitative assay kit (Nanjing Jiancheng Bioengineering Institute, China), and all data for antioxidative indicators were normalized to the total protein content. Meanwhile, 100% acetone was used for extracting Chl *a* in a 24-hour dark period at − 20 °C according to the method of Zhang et al. [7]. The homogenate was centrifuged using Sigma 3-18KS freezing centrifuge (Sigma Laborzentrifugen GmbH, Germany) at 4,000 rpm for 10 min; the supernatant was collected, and the absorbance was measured at OD630 and OD663 using a UV-2700 spectrophotometer (SHIMADZU, Japan). The chlorophyll content was computed using the equations in Jeffrey and Humphrey [85]. The coral antioxidant-related indices and the Chl *a* content were analyzed. Pairwise group comparisons were performed using t-tests, and *p*-values were adjusted for multiple testing via Bonferroni correction, with $p < 0.05$ representing a significant difference and $p < 0.01$ representing a highly significant difference.

DNA extraction, 16S rRNA gene amplicon sequencing, and data analysis

Small amounts (2–4 g) of each coral sample were crushed with a mortar and pestle, and DNA was extracted using the TIANamp Marine Animals DNA Kit (Tiangen, China). Finally, the high-quality DNA of 15 samples from three groups was extracted. PCR amplification was performed using the primers 338 F (5′-ACTCCTACGGGAGGCAGCAG-3′) and 806R (5′-GGACTACHVGGGTWTCTAAT-3′) for the V3V4 variable region of bacterial 16S rRNA with an ABI GeneAmp 9700 thermal cycler (Thermo Fisher Scientific, USA), followed by detection and quantification of the PCR products. A TruSeq™ DNA Sample Prep Kit (Illumina, USA) was used to prepare Illumina libraries, which were then sequenced on an Illumina MiSeq platform following standard protocols.

The raw data were split according to the samples and then quality-filtered and merged using the Trimmomatic read trimming tool and FLASH [84]. The resulting high-quality reads were denoised using Qiime2 (Version 2023.5.0) via the DADA2 plugin to obtain amplicon sequence variants (ASVs) [86]. All sequences annotated as being from chloroplasts and mitochondria were removed to ensure the purity of the data, and the remaining sequences were normalized by the lowest number of sequences. To quantify fluctuations in bacterial species, the values of alpha diversity indices (Ace, Chao, Sobs, Shannon, and Simpson) were calculated using Mothur (https://mothur.org/), and the data were analyzed using the Kruskal-Wallis H test [87]. Sample spacing of beta diversity was calculated using principal coordinate analysis (PCoA) based on the weighted

Bray-Curtis algorithm in order to visualize the community structure between samples. Linear discriminant analysis effect size (LEfSe; http://huttenhower.sph.harvard.edu/galaxy/root?tool_id=lefse_upload) was used to profile the species characteristics that explained most of the differences between groups with a linear discriminant analysis (LDA) threshold of 4 and a p-value < 0.05. The data were analyzed through the free online platform of majorbio cloud platform (http://cloud.majorbio.com) [88].

RNA extraction, transcriptome sequencing, and data analysis

The coral total RNA was extracted from four samples per group using a TRIzol™ Plus RNA Purification Kit (Thermo Fisher Scientific, USA) according to the manufacturer's instructions. Oligo (dT) magnetic beads were used to enrich the mRNA. An Illumina Stranded mRNA Prep Ligation Kit (Illumina, USA) was then used to construct a library. Sequencing was performed using an Illumina NovaSeq 6000 according to standard protocols.

Clean reads were obtained after adapter removal, pruning, and filtering of raw reads via Fastp (https://github.com/OpenGene/fastp) [89]. All clean reads were assembled *de novo* by Trinity (https://github.com/trinityrnaseq/trinityrnaseq/wiki) [26]. BLASTx was used to obtain the sequences from the coral hosts, according to Yu et al. [6]. The sequences were annotated using non-redundant (Nr; Version 2022.10), Gene Ontology (GO; Version 2022.0915), and Kyoto Encyclopedia of Genes and Genomes (KEGG; Version 2022.10) databases. To measure the transcription and gene expression levels, RSEM (version 1.3.3) was used and the transcripts per million (TPM) was applied. To further determine whether the groups had genetic differences, the AMOVA analysis of the SNP sites in the transcript data was performed using Arlequin (Version 3.5.2.2). The samples were clustered based on the expression of unigenes by principal component analysis (PCA), followed by the identification of differentially expressed unigenes (DEGs) using DESeq2 (Version 1.24.0) with a false discovery rate (FDR) < 0.01 and an absolute value of $\log_2$FC ≥ 1. To further explore the DEGs, information regarding function and pathways was obtained by GO and KEGG annotation. The KEGG enrichment analyses was carried out using majorbio cloud platform [88] with Python package scipy, and used Fisher's exact test and $p < 0.05$ as the criteria for significant judgment. To avoid result narrowing due to overcorrection, no multiple testing correction was applied to enrichment analyses, but the FDR values, corrected using the Benjamini-Hochberg method, are still provided in Additional File 5 for the reader's reference. Enrichment network analysis was performed based on the relationship between significant KEGG pathways to obtain the major pathways, and then key DEGs were screened by the most dominant and representative pathway mechanism.

Extraction and identification of metabolites

A total of 24 samples (eight samples per group) were employed to extract the metabolites. First, a small amount of each coral sample (100 ± 5 mg) was added to a mortar, and metabolite extraction was performed using 400 µL of methanol-water extraction solution (4:1, v/v) containing 0.02 mg/mL of internal standard (L-2-chlorophenylalanine). Samples were ground by the Wonbio-96c frozen tissue grinder (Shanghai wanbo biotechnology, China) for 6 min at − 10 °C, followed by low-temperature ultrasonic extraction for 30 min at 5 °C. The samples were then allowed to left at − 20 °C for 30 min, and centrifuged using Centrifuge 5430R (Eppendorf, Germany) at 11,500 rpm for 10 min. Finally, the supernatant was collected. Equal volumes of all sample supernatant were taken and mixed to prepare quality control samples (QC), and a QC was included in every eight samples during instrumental analysis. All supernatant were analyzed by LC-MS using a UHPLC-Q Exactive HF-X system (Thermo Fisher Scientific, USA) with the following conditions. An ACQUITY UPLC HSS T3 column (100 mm × 2.1 mm i.d., 1.8 µm; Waters, USA) was used for extraction. Mobile phase A consisted of 95% water and 5% acetonitrile (with 0.1% formic acid), and mobile phase B consisted of 47.5% acetonitrile, 47.5% isopropanol, and 5% water (with 0.1% formic acid). The injection volume was 3 µL, and the column temperature was 40 °C. The samples were ionized by electrospray, the specific parameters of the mass spectra were as follows. Sheath gas flow rate was set to 50 arb and aux gas flow rate was 13 arb. Spray voltage was 3,500 in positive mode and 3,500 in negative mode. Normalized collision energy was 20 eV, 40 eV, 60 eV. Full MS resolution was 60,000, and MS/MS resolution was 7500. Scan type was 70–1050 m/z. The mass spectral signals were collected in positive (POS) and negative (NEG) ion scanning modes. Then, the raw data were imported into Progenesis QI (Waters, USA) for baseline filtering, peak identification, integration, retention time correction, and peak alignment. Finally, a data matrix of retention time, mass-to-charge ratio, and peak intensity was obtained, which was then matched according to the HMDB (https://hmdb.ca/) and Metlin (https://metlin.scripps.edu/) databases.

Before analyzing the data, the data matrix was preprocessed by removing and filling in missing values. Specifically, only those metabolic features with non-zero values in at least 80% of the samples in any set were preserved. The empty values are then filled using the smallest value in the original matrix. The mass spectrometry peak intensities corresponding to all metabolic features were normalized using the sum normalization method.

Variables with a relative standard deviation > 30% in QC were removed, and the remaining variables were log transformed. Partial least squares discriminant analysis (PLS-DA) was used to examine group differences. The Ropls package in R (Version 1.6.2) was used to perform the OPLS-DA. Further, metabolites from POS and NEG modes were combined for significantly different metabolite (DM) identification and further analysis. DMs were identified based on the value of variable importance in the projection (VIP) obtained from the orthogonal partial least squares discriminant analysis (OPLS-DA) model and FDR from Student's *t*-test. Metabolites with FDR < 0.01 and VIP > 1 were defined as DMs. DMs were matched to the KEGG database and analyzed for enrichment using the Python package scipy.stats, and the *p*-values were obtained by Fisher's exact test. Similar to the transcriptomic analysis, to prevent the narrowing of results from overcorrection, multiple testing correction was not applied to the enrichment analyses. KEGG pathway analysis was performed based on the relative-betweenness centrality of the topology. The metabolomics data analysis was performed using the free online platform of majorbio cloud platform (http://cloud.majorbio.com) [88].

Association analyses and statistics

To determine whether gene expression levels and metabolite abundances were correlated, a credible O2PLS model was applied to fit two omics datasets [90, 91] according to the description in Bouhaddani et al. [92]. The DEGs were designated as the X dataset, and the DMs were defined as the Y dataset. For assessing the explanatory ability of the two datasets, the contribution values (R^2X and R^2Y) were output separately. Significantly enriched KEGG pathways were screened in both transcriptomics and metabolomics. First, pathways were selected with first category as metabolism. Then, among the pathways in the first category of cellular processes, the innate immune pathways that have been reported in corals [55] were selected. Finally, DEGs from these pathways and DM were correlated. Spearman correlation coefficients and the significance of gene expression and metabolite abundances were calculated based on the overall determination of the correlation between the two omics with the O2PLS model. The integrative model diagram was created by BioRender (https://biorender.com) and Adobe Illustrator 2020 (Adobe, USA).

Supplementary Information

The online version contains supplementary material available at https://doi.org/10.1186/s12864-025-11660-4.

Supplementary Material 1

Supplementary Material 2

Supplementary Material 3

Supplementary Material 4

Supplementary Material 5

Supplementary Material 6

Supplementary Material 7

Supplementary Material 8

Supplementary Material 9

Supplementary Material 10

Acknowledgements

We thank the staff of the Weizhou Island Coral Museum of Guangxi University for their assistance and support in this study. We thank the experts who edited and reviewed this paper for publication.

Author contributions

Study conception: MZ; Field work: LL; Lab work: SH; Data Curation: MZ, SH; Writing-Original Draft: MZ, SH; Writing-Review & Editing: MZ, SH, KY; Visualization: SH; Supervision: MZ; Project Administration: MZ; Funding Acquisition: KY.

Funding

This work was supported by National Natural Science Foundation of China (No. 42030502), Guangxi Science and Technology Program (No. AD25069075), National Natural Science Foundation of China (No. 42090041).

Data availability

The raw 16S rRNA gene amplicon sequencing data have been submitted to the NCBI Sequence Read Archive (SRA) database (BioProject ID: PRJNA1049633). The raw data generated from RNA sequencing could be found in the BioProject (PRJNA1041081) at the NCBI SRA database. The data matrix of metabolomics has been uploaded to MetaboLights (MTBLS8982).

Declarations

Ethics approval and consent to participate

The animal trial was carried out at the Guangxi Laboratory on the Study of Coral Reefs in the South China Sea and approved by the ethical review committee for animal project in Guangxi University.

Consent for publication

Not applicable.

Competing interests

The authors declare no competing interests.

Author details

[1]Guangxi Laboratory on the Study of Coral Reefs in the South China Sea, Coral Reef Research Center of China, School of Marine Sciences, Guangxi University, Nanning 530004, PR China
[2]Southern Marine Science and Engineering Guangdong Laboratory (Guangzhou), Guangzhou 511458, PR China

Received: 14 August 2024 / Accepted: 30 April 2025
Published online: 14 May 2025

References

1. Spalding M, Burke L, Wood SA, Ashpole J, Hutchison J. zu Ermgassen P. Mapping the global value and distribution of coral reef tourism. Mar Policy. 2017;82:104–13.
2. Bourne DG, Morrow KM, Webster NS. Insights into the coral microbiome: underpinning the health and resilience of reef ecosystems. Annu Rev Microbiol. 2016;70:317–40.

3. Huang W, Yang E, Yu K, Meng L, Wang Y, Liang J, et al. Lower cold tolerance of tropical *Porites lutea* is possibly detrimental to its migration to relatively high latitude refuges in the South China sea. Mol Ecol. 2022;31:5339–55.
4. Rädecker N, Pogoreutz C, Gegner HM, Cardenas A, Roth F, Bougoure J, et al. Heat stress destabilizes symbiotic nutrient cycling in corals. Proc Natl Acad Sci USA. 2021;118:e2022653118.
5. Sully S, Burkepile DE, Donovan MK, Hodgson G, van Woesik R. A global analysis of coral bleaching over the past two decades. Nat Commun. 2019;10:1264.
6. Yu X, Yu K, Chen B, Liao Z, Liang J, Yao Q, et al. Different responses of scleractinian coral *Acropora pruinosa* from Weizhou Island during extreme high temperature events. Coral Reefs. 2021;40:1697–711.
7. Zhang Y, Ip JC, Xie JY, Yeung YH, Sun Y, Qiu JW. Host-symbiont transcriptomic changes during natural bleaching and recovery in the leaf coral *Pavona decussata*. Sci Total Environ. 2022;806:150656.
8. Perry CT, Larcombe P. Marginal and non-reef-building coral environments. Coral Reefs. 2003;22:427–32.
9. Röthig T, Bravo H, Corley A, Prigge T-L, Chung A, Yu V, et al. Environmental flexibility in *Oulastrea crispata* in a highly urbanised environment: a microbial perspective. Coral Reefs. 2020;39:649–62.
10. Guest JR, Low J, Tun K, Wilson B, Ng C, Raingeard D, et al. Coral community response to bleaching on a highly disturbed reef. Sci Rep. 2016;6:20717.
11. Brown NP, Forsman ZH, Tisthammer KT, Richmond RH. A resilient brooding coral in the broadcast spawning *Porites lobata* species complex: a new endemic, introduced species, mutant, or new adaptive potential? Coral Reefs. 2020;39:809–18.
12. Barros Y, Lucas CC, Soares MO. An urban intertidal reef is dominated by fleshy macroalgae, sediment, and bleaching of a resilient coral (*Siderastrea stellata*). Mar Pollut Bull. 2021;173:112967.
13. Castrillón-Cifuentes AL, Lozano-Cortés DF, Zapata FA. Effect of short-term subaerial exposure on the cauliflower coral, *Pocillopora damicornis*, during a simulated extreme low-tide event. Coral Reefs. 2017;36:401–14.
14. Alina DN, Rachmawati R, Zamani NP, Madduppa H. Exposure at low tide leads to a different microbial abundance of intertidal coral *Acropora pulchra*. Mar Biol Res. 2022;18:520–30.
15. Raymundo LJ, Burdick D, Lapacek VA, Miller R, Brown V. Anomalous temperatures and extreme tides: Guam Staghorn *Acropora* succumb to a double threat. Mar Ecol Prog Ser. 2017;564:47–55.
16. Speelman PE, Parger M, Schoepf V. Divergent recovery trajectories of intertidal and subtidal coral communities highlight habitat-specific recovery dynamics following bleaching in an extreme macrotidal reef environment. PeerJ. 2023;11:e15987.
17. Jung EMU, Stat M, Thomas L, Koziol A, Schoepf V. Coral host physiology and symbiont dynamics associated with differential recovery from mass bleaching in an extreme, macro-tidal reef environment in Northwest Australia. Coral Reefs. 2021;40:893–905.
18. Anthony KRN, Kerswell AP. Coral mortality following extreme low tides and high solar radiation. Mar Biol. 2007;151:1623–31.
19. Pandolfi JM, Kiessling W. Gaining insights from past reefs to inform Understanding of coral reef response to global climate change. Curr Opin Env Sust. 2014;7:52–8.
20. Hoegh-Guldberg O, Fine M, Skirving W, Johnstone R, Dove S, Strong A. Coral bleaching following wintry weather. Limnol Oceanogr. 2005;50:265–71.
21. Modys AB, Oleinik AE, Toth LT, Precht WF, Mortlock RA. Modern coral range expansion off Southeast Florida falls short of late holocene baseline. Commun Earth Environ. 2024;5:119.
22. Huang W, Meng L, Xiao Z, Tan R, Yang E, Wang Y, et al. Heat-tolerant intertidal rock pool coral *Porites lutea* can potentially adapt to future warming. Mol Ecol. 2024;33:e17273.
23. Shiu J-H, Keshavmurthy S, Chiang P-W, Chen H-J, Lou S-P, Tseng C-H, et al. Dynamics of coral-associated bacterial communities acclimated to temperature stress based on recent thermal history. Sci Rep. 2017;7:14933.
24. Ziegler M, Seneca FO, Yum LK, Palumbi SR, Voolstra CR. Bacterial community dynamics are linked to patterns of coral heat tolerance. Nat Commun. 2017;8:14213.
25. Roach TNF, Dilworth J, Jones HCM, Quinn AD, Drury RA. Metabolomic signatures of coral bleaching history. Nat Ecol Evol. 2021;5:495–503.
26. Yu X, Yu K, Liao Z, Chen B, Qin Z, Liang J, et al. Adaptation strategies of relatively high-latitude marginal reef corals in response to severe temperature fluctuations. Sci Total Environ. 2023;903:166439.
27. Cheng CM, Cheng YR, Ding DS, Chen YT, Sun WT, Pan CH. Effects of ciliate infection on the activities of two antioxidant enzymes (SOD and CAT) in captive coral (*Goniopora columna*) and evaluation of drug therapy. Biol. 2021;10:1216.
28. Zhang Y, Chen RW, Liu X, Zhu M, Li Z, Wang A, et al. Oxidative stress, apoptosis, and transcriptional responses in *Acropora microphthalma* under simulated diving activities. Mar Pollut Bull. 2022;183:114084.
29. Chen YT, Ding DS, Lim YC, Singhania RR, Hsieh S, Chen CW, et al. Impact of polyethylene microplastics on coral *Goniopora columna* causing oxidative stress and histopathology damages. Sci Total Environ. 2022;828:154234.
30. Stambler N, Dubinsky Z. Stress effects on metabolism and photosynthesis of hermatypic corals. In: Rosenberg E, Loya Y, editors. Coral health and disease. Berlin, Heidelberg: Springer Berlin Heidelberg; 2004. pp. 195–215.
31. Rosenberg E, Koren O, Reshef L, Efrony R, Zilber-Rosenberg I. The role of microorganisms in coral health, disease and evolution. Nat Rev Microbiol. 2007;5:355–62.
32. Patel NP, Shimpi GG, Haldar S. A comparative account of resistance and antagonistic activity of healthy and bleached coral-associated bacteria as an indicator of coral health status. Ecol Indic. 2021;120:106886.
33. Han S, Cheng X, Wang T, Li X, Cai Z, Zheng H, et al. AI-2 quorum sensing signal disrupts coral symbiotic homeostasis and induces host bleaching. Environ Int. 2024;188:108768.
34. Hsieh YE, Lu C-Y, Liu P-Y, Kao J-M, Yang S-Y, Wu C-Y, et al. Successive responses of three coral holobiont components (coral hosts, symbiotic algae, and bacteria) to daily temperature fluctuations. Ecol Indic. 2024;158:111515.
35. Hernandez-Agreda A, Gates RD, Ainsworth TD. Defining the core Microbiome in corals' microbial soup. Trends Microbiol. 2017;25:125–40.
36. Röthig T, Ochsenkühn MA, Roik A, van der Merwe R, Voolstra CR. Long-term salinity tolerance is accompanied by major restructuring of the coral bacterial Microbiome. Mol Ecol. 2016;25:1308–23.
37. Ahmed HI, Herrera M, Liew YJ, Aranda M. Long-term temperature stress in the coral model *Aiptasia* supports the Anna karenina principle for bacterial microbiomes. Front Microbiol. 2019;10:975.
38. Mohamed AR, Ochsenkühn MA, Kazlak AM, Moustafa A, Amin SA. The coral microbiome: towards an Understanding of the molecular mechanisms of coral-microbiota interactions. FEMS Microbiol Rev. 2023;47:fuad005.
39. Oh HM, Kang I, Ferriera S, Giovannoni SJ, Cho JC. Genome sequence of the oligotrophic marine gammaproteobacterium HTCC2143, isolated from the Oregon Coast. J Bacteriol. 2010;192:4530–1.
40. Hu X, Su H, Zhang P, Chen Z, Xu Y, Xu W, et al. Microbial community structure and metabolic characteristics of intestine and gills of dwarf-form populations of *Sthenoteuthis oualaniensis* in South China sea. Fishes. 2022;7:191.
41. van de Water JAJM, Voolstra CR, Rottier C, Cocito S, Peirano A, Allemand D, et al. Seasonal stability in the microbiomes of temperate gorgonians and the red coral *Corallium rubrum* across the mediterranean sea. Microb Ecol. 2017;75:274–88.
42. Zheng N, Ding N, Gao P, Han M, Liu X, Wang J, et al. Diverse algicidal bacteria associated with harmful bloom-forming *Karenia Mikimotoi* in estuarine soil and seawater. Sci Total Environ. 2018;631–2:1415–20.
43. Varasteh T, Hamerski L, Tschoeke D, Lima AS, Garcia G, Cosenza CAN, et al. Conserved pigment profiles in phylogenetically diverse symbiotic bacteria associated with the corals *Montastraea cavernosa* and *Mussismilia braziliensis*. Microb Ecol. 2020;81:267–77.
44. García-Romero I, Pérez-Pulido AJ, González-Flores YE, Reyes-Ramírez F, Santero E, Floriano B. Genomic analysis of the nitrate-respiring *Sphingopyxis granuli* (formerly *Sphingomonas macrogoltabida*) strain TFA. BMC Genomics. 2016;17:93.
45. Huang S, Luo L, Wen B, Liu X, Yu K, Zhang M. Metabolic signatures of two scleractinian corals from the Northern South China sea in response to extreme high temperature events. Mar Environ Res. 2024;198:106490.
46. Zhang M, Huang S, Luo L, Yu X, Wang H, Yu K, et al. Insights into the molecular mechanisms underlying the different heat tolerance of the scleractinian coral *Pavona decussata*. Coral Reefs. 2024;43:429–42.
47. MacLean A, Legendre F, Appanna VD. The Tricarboxylic acid (TCA) cycle: a malleable metabolic network to counter cellular stress. Crit Rev Biochem. 2023;58:81–97.
48. da Silva Fonseca J, de Barros Marangoni LF, Marques JA, Bianchini A. Energy metabolism enzymes Inhibition by the combined effects of increasing temperature and copper exposure in the coral *Mussismilia harttii*. Chemosphere. 2019;236:124420.
49. Yang D, Tang Y, Zhu B, Pang H, Rong X, Gao Y, et al. Engineering cell membrane-cloaked catalysts as multifaceted artificial peroxisomes for biomedical applications. Adv Sci. 2023;10:2206181.

50. Kapetanou M, Athanasopoulou S, Gonos ES. Transcriptional regulatory networks of the proteasome in mammalian systems. IUBMB Life. 2021;74:41–52.
51. Porro B, Zamoum T, Forcioli D, Gilson E, Poquet A, Di Franco E, et al. Different environmental response strategies in sympatric corals from Pacific Islands. Commun Earth Environ. 2023;4:311.
52. Maiuri MC, Zalckvar E, Kimchi A, Kroemer G. Self-eating and self-killing: crosstalk between autophagy and apoptosis. Nat Rev Mol Cell Biol. 2007;8:741–52.
53. Majerova E, Carey FC, Drury C, Gates RD. Preconditioning improves bleaching tolerance in the reef-building coral *Pocillopora acuta* through modulations in the programmed cell death pathways. Mol Ecol. 2021;30:3560–74.
54. Filomeni G, De Zio D, Cecconi F. Oxidative stress and autophagy: the clash between damage and metabolic needs. Cell Death Differ. 2015;22:377–88.
55. Mansfield KM, Gilmore TD. Innate immunity and cnidarian-Symbiodiniaceae mutualism. Dev Comp Immunol. 2019;90:199–209.
56. Fuess LE, Pinzón CJH, Weil E, Grinshpon RD, Mydlarz LD. Life or death: disease-tolerant coral species activate autophagy following immune challenge. Proc R Soc B. 2017;284:20170771.
57. Massagué J, Sheppard D. TGF-β signaling in health and disease. Cell. 2023;186:4007–37.
58. Pei JY, Yu WF, Zhang JJ, Kuo TH, Chung HH, Hu JJ, et al. Mass spectrometry-based metabolomic signatures of coral bleaching under thermal stress. Anal Bioanal Chem. 2022;414:7635–46.
59. Biscéré T, Ferrier-Pagès C, Grover R, Gilbert A, Rottier C, Wright A, et al. Enhancement of coral calcification via the interplay of nickel and urease. Aquat Toxicol. 2018;200:247–56.
60. Crandall JB, Teece MA. Urea is a dynamic pool of bioavailable nitrogen in coral reefs. Coral Reefs. 2011;31:207–14.
61. Grover R, Maguer JF, Allemand D, Ferrier-Pagès C. Urea uptake by the scleractinian coral *Stylophora pistillata*. J Exp Mar Biol Ecol. 2006;332:216–25.
62. Crossland CJ, Barnes DJ. The role of metabolic nitrogen in coral calcification. Mar Biol. 1974;28:325–32.
63. Muthukumaran S, Jaidev J, Umashankar V, Sulochana KN. Ornithine and its role in metabolic diseases: an appraisal. Biomed Pharmacother. 2017;86:185–94.
64. Courtney TA, Lebrato M, Bates NR, Collins A, de Putron SJ, Garley R, et al. Environmental controls on modern scleractinian coral and reef-scale calcification. Sci Adv. 2017;3:e1701356.
65. Vajed Samiei J, Saleh A, Mehdinia A, Shirvani A, Kayal M. Photosynthetic response of Persian Gulf acroporid corals to summer versus winter temperature deviations. PeerJ. 2015;3:e1062.
66. Kuffner IB, Hickey TD, Morrison JM. Calcification rates of the massive coral *Siderastrea siderea* and crustose coralline algae along the Florida keys (USA) outer-reef tract. Coral Reefs. 2013;32:987–97.
67. Marshall AT, Clode P. Calcification rate and the effect of temperature in a zooxanthellate and an azooxanthellate scleractinian reef coral. Coral Reefs. 2004;23:218–24.
68. Sikorskaya TV. Coral lipidome: molecular species of phospholipids, glycolipids, betaine lipids, and sphingophosphonolipids. Mar Drugs. 2023;21:335.
69. Imbs AB, Dang LTP. Seasonal dynamics of fatty acid biomarkers in the soft coral *Sinularia flexibilis*, a common species of Indo-Pacific coral reefs. Biochem Syst Ecol. 2021;96:104246.
70. Rocker MM, Francis DS, Fabricius KE, Willis BL, Bay LK. Temporal and Spatial variation in fatty acid composition in *Acropora tenuis* corals along water quality gradients on the great barrier reef, Australia. Coral Reefs. 2019;38:215–28.
71. Wei J, Chen S, Guo W, Feng B, Yang S, Huang C, et al. Leukotriene D4 induces cellular senescence in osteoblasts. Int Immunopharmacol. 2018;58:154–9.
72. Torda G, Donelson JM, Aranda M, Barshis DJ, Bay L, Berumen ML, et al. Rapid adaptive responses to climate change in corals. Nat Clim Change. 2017;7:627–36.
73. Hernandez-Agreda A, Leggat W, Bongaerts P, Ainsworth TD. The microbial signature provides insight into the mechanistic basis of coral success across reef habitats. mBio. 2016;7:e00560–16.
74. Yu X, Yu K, Chen B, Liao Z, Huang W. Nanopore long-read RNAseq reveals regulatory mechanisms of thermally variable reef environments promoting heat tolerance of scleractinian coral *Pocillopora damicornis*. Environ Res. 2021;195:110782.
75. Sáez GT, Están-Capell N. Antioxidant enzymes. In: Schwab M, editor. Encyclopedia of Cancer. Berlin, Heidelberg: Springer; 2014.
76. Ginguay A, Cynober LA. Amino acids| amino acid metabolism. In: Jez J, editor. Encyclopedia of biological chemistry III (Third Edition). Oxford: Elsevier; 2021. pp. 2–9.
77. Cohen GN. The aspartic acid family of amino acids. Biosynthesis. Microbial biochemistry. Dordrecht: Springer; 2004.
78. Keighan R, van Woesik R, Yalon A, Nam J, Houk P. Moderate chlorophyll-*a* environments reduce coral bleaching during thermal stress in Yap, Micronesia. Sci Rep. 2023;13:9338.
79. Dandan SS, Falter JL, Lowe RJ, McCulloch MT. Resilience of coral calcification to extreme temperature variations in the Kimberley region, Northwest Australia. Coral Reefs. 2015;34:1151–63.
80. Marshall PA, Baird AH. Bleaching of corals on the great barrier reef: differential susceptibilities among taxa. Coral Reefs. 2000;19:155–63.
81. Loya Y, Sakai K, Yamazato K, Nakano Y, Sambali H, van Woesik R. Coral bleaching: the winners and the losers. Ecol Lett. 2001;4:122–31.
82. Buckee J, Hetzel Y, Edge W, Verduin J, Pattiaratchi C. Daily timing of low tide drives seasonality in intertidal emersion mortality risk. Front Mar Sci. 2022;9:904191.
83. Hoarau L, Mouquet P, Ropert M, Cuvillier A, Massé L, Bonhommeau S, et al. Negative sea level anomalies with extreme low tides in the South-West Indian ocean shape reunion Island's fringing coral reef flats. Ecol Indic. 2023;154:110508.
84. Yu X, Yu K, Huang W, Liang J, Qin Z, Chen B, et al. Thermal acclimation increases heat tolerance of the scleractinian coral *Acropora pruinosa*. Sci Total Environ. 2020;733:139319.
85. Jeffrey SW, Humphrey GF. New spectrophotometric equations for determining chlorophylls *a*, *b*, c_1 and c_2 in higher plants, algae and natural phytoplankton. Biochemie Und Physiologie Der Pflanzen. 1975;167:191–4.
86. Bolyen E, Rideout JR, Dillon MR, Bokulich NA, Abnet CC, Al-Ghalith GA, et al. Reproducible, interactive, scalable and extensible Microbiome data science using QIIME 2. Nat Biotechnol. 2019;37:852–7.
87. Kruskal WH, Wallis WA. Use of ranks in one-criterion variance analysis. J Am Stat Assoc. 1952;47:583–621.
88. Ren Y, Guo Y, Shi C, Liu L, Guo Q, Han C, et al. Majorbio cloud: A one-stop, comprehensive bioinformatic platform for multiomics analyses. iMeta. 2022;1:e12.
89. Chen S, Zhou Y, Chen Y, Gu J. Fastp: an ultra-fast all-in-one FASTQ preprocessor. Bioinform. 2018;34:i884–90.
90. Bouhaddani SE, Houwing-Duistermaat J, Salo P, Perola M, Jongbloed G, Uh H-W. Evaluation of O2PLS in omics data integration. BMC Bioinform. 2016;17:S11.
91. Trygg J, Wold S. O2-PLS, a two-block (X-Y) latent variable regression (LVR) method with an integral OSC filter. J Chemom. 2003;17:53–64.
92. Bouhaddani SE, Uh H-W, Jongbloed G, Hayward C, Klarić L, Kiełbasa SM, et al. Integrating omics datasets with the OmicsPLS package. BMC Bioinform. 2018;19:371.

Publisher's note